



ELSEVIER

Available online at www.sciencedirect.com

SCIENCE @ DIRECT®

Finite Elements in Analysis and Design 39 (2003) 765–782

FINITE ELEMENTS
IN ANALYSIS
AND DESIGN

www.elsevier.com/locate/finel

Homogenization of magnetostrictive particle-filled elastomers using an interface-enriched reproducing kernel particle method

Dongdong Wang^a, Jiun-Shyan Chen^{a,*}, Lizhi Sun^b

^a*Department of Civil & Environmental Engineering, University of California, 5731G Boelter Hall, Los Angeles, CA 90095-1593, USA*

^b*Department of Civil & Environmental Engineering, The University of Iowa, Iowa City, IA 52242-1527, USA*

Received 22 October 2002; accepted 22 October 2002

Abstract

A formulation is proposed for homogenization of magnetostrictive particle-filled elastomers (MPFE) based on an interface-enriched reproducing kernel particle method. A variational equation for obtaining the local fluctuating deformation of MPFE is introduced. The magnetostrictive effect in the metal inclusion is modeled as an eigen-deformation. An interface-enriched reproducing kernel approximation with embedded derivative discontinuities on the material interface is presented. This approach does not require additional degrees of freedom in the approximation of displacement field for the interface conditions compared to the conventional reproducing kernel approximation. Microscopic solution and homogenized constitutive behavior of uniaxial tension and simple shear deformation of MPFE are presented.

© 2003 Elsevier Science B.V. All rights reserved.

Keywords: Magnetostrictive particle-filled elastomer (MPFE); Reproducing kernel approximation; Homogenization; Meshfree method

1. Introduction

The magnetostrictive particle-filled elastomer (MPFE) is a new class of smart material that exhibits sound mechanical properties under the magnetic field and thus allows an active control of spring rate for vibration isolation applications [1,2]. Micromechanics-based approaches [3] have been employed to estimate the overall properties of magnetostrictive particle-reinforced composites [4,5] undergoing small deformation. Studies also have been undertaken for the particle-filled elastomers without magnetostrictive effect [6,7].

* Corresponding author.

E-mail addresses: jschen@seas.ucla.edu (J.-S. Chen), lzsun@engineering.uiowa.edu (L. Sun).

In composite materials, the effective properties may be obtained by finite element based strain- and stress-control homogenization methods for linear [8–10] and nonlinear [11–18] problems. Generally, the finite element discretization of heterogeneous material unit cell requires matching elements along the material interface. In the case of MPFE, due to the large difference in the constituent moduli, the much softer rubber component undergoes relatively large and complex deformation compared to the metal particles. This increases the complexity in constructing the matched mesh along the material interfaces that meets the resolution requirement of the two constituents. Localized large deformation in the rubber component is an additional challenge to the finite element based analysis.

In this paper a Galerkin meshfree method is proposed for effective large deformation analysis of MPFE microstructure. Meshfree methods such as element free Galerkin (EFG) [20,21], reproducing kernel particle method (RKPM) [22–25], partition of unity method (PUM) [26,27], and HP clouds [28,29] employ smooth meshfree shape functions with overlapping supports that cannot properly represent jump conditions across the material interface. Methods have been proposed to model the material interfaces under the meshfree framework by introducing interface jump conditions in the weak form of meshfree discretization via a Lagrange multiplier method [30] or by enriching special jump functions in the meshfree shape functions [31]. In both approaches, additional degrees of freedom are introduced in the approximation of displacements, which result in a larger discrete system.

In this study, we first present a variational formulation for homogenization of MPFE under large deformation. Since the ferromagnetic Fe particle inclusion under magnetic field leads to a dimension change, an eigen-deformation in the unit microstructure is introduced to account for this effect. The microscopic deformation of MPFE is composed of external macroscopic deformation, locally periodic fluctuating deformation, and the deformation associated with internal eigen-deformation.

The discretization of MPFE variational homogenization equation is performed using an interface-enriched reproducing kernel particle method (I-RKPM). We formulated I-RKPM by coupling the reproducing kernel shape function and an interface enrichment function via the reproducing conditions. Compared to earlier work [30,31], this approach does not introduce additional degrees of freedom in the approximation of displacements. Using the proposed method, we analyzed the effective nonlinear stress–strain relations of MPFE in tension and simple shear, and also studied the effect of magnetostrictive eigen-deformation on the overall stress–strain behavior of MPFE.

This paper is organized as follows. The kinematics of MPFE unit microstructure and MPFE homogenization equation are presented in Section 2. Section 3 introduces an I-RKPM with embedded interface conditions for the discretization of MPFE microstructure. In Section 4, meshfree discretization of MPFE homogenization equation is presented. Finally, we conduct microscopic analyses and homogenization of MPFE in Section 5, followed by concluding remarks in Section 6.

2. Variational homogenization equation of MPFE microstructure

2.1. MPFE microstructure kinematics in 2-dimension

Homogenization is the process of taking a heterogeneous microscale field and finding its effective properties at a macroscale. If the variation of a field function f (such as strain, stress) in the microstructure is much larger than the wavelengths λ_i of the microstructure, the field f in the

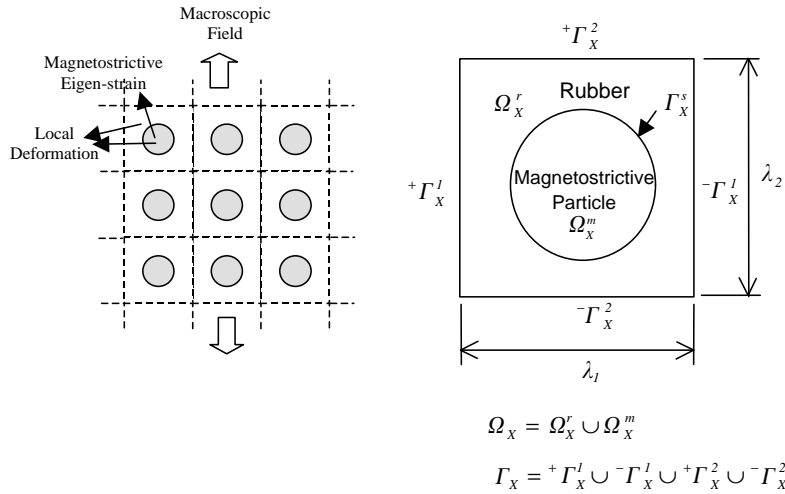


Fig. 1. Microstructure of MPFE.

2-dimensional microstructure is assumed λ_i -periodic, such that

$$f(X_1, X_2) = f(X_1 + n_1\lambda_1, X_2 + n_2\lambda_2), \tag{2.1}$$

where n_1, n_2 are small arbitrary integers, λ_1, λ_2 are the microstructure wavelengths in two directions, and X_1, X_2 are the material coordinates defined in the microstructure.

With the consideration of λ_i -periodicity in Eq. (2.1), a MPFE unit microstructure as shown in Fig. 1 is defined in the undeformed configuration as

$$\Omega_X = \prod_{i=1}^2]0, \lambda_i[, \tag{2.2}$$

where $\Omega_X = \Omega_X^r \cup \Omega_X^m$ is the material domain of MPFE, while Ω_X^r and Ω_X^m denote the material domains of rubber and magnetostriuctive particle, respectively. The boundary of the MPFE unit microstructure, $\Gamma_X = +\Gamma_X^1 \cup -\Gamma_X^1 \cup +\Gamma_X^2 \cup -\Gamma_X^2$, is the union of surface pairs $\{+\Gamma_X^i, -\Gamma_X^i\}_{i=1}^2$ in each i -direction. The interface of rubber and the magnetostriuctive particle is denoted as Γ_X^s in the material domain. In the microstructure, the deformation gradient is defined by

$$\mathbf{F} = \frac{\partial \mathbf{x}}{\partial \mathbf{X}} = \mathbf{1} + \frac{\partial \mathbf{u}}{\partial \mathbf{X}}, \tag{2.3}$$

where \mathbf{x} is the microscale spatial coordinate, $\mathbf{1}$ is the 2nd rank identity tensor, \mathbf{u} is the microscale displacement field, and the microscale deformation gradient is λ_i -periodic:

$$\mathbf{F}(X_1, X_2) = \mathbf{F}(X_1 + n_1\lambda_1, X_2 + n_2\lambda_2). \tag{2.4}$$

The periodicity of the deformation field in the microscale suggests that it admits additive decompositions into (1) macroscale contributions which are constant on the microscale, and (2) purely oscillatory contributions which can vary quite significantly on the microscale. Further considering

the magnetostrictive eigen-deformation, $\mathbf{F}(\mathbf{X})$ in the MPFE microstructure can be expressed as

$$\mathbf{F}(\mathbf{X}) = \bar{\mathbf{F}} - \mathbf{F}^0 + \mathbf{F}^*(\mathbf{X}), \tag{2.5}$$

where $\bar{\mathbf{F}}$ is the macroscale deformation, \mathbf{F}^* is the locally periodic fluctuating deformation which can vary quite significantly on the microscale, and \mathbf{F}^0 represents the magnetostrictive eigen-deformation of ferromagnetic particle inclusion which is assumed to be constant in the inclusion. The local deformation \mathbf{F}^* results from the local heterogeneity of microstructure, and it can be shown that

$$\langle \mathbf{F}(\mathbf{X}) \rangle_{\Omega_X} = \bar{\mathbf{F}} - \mathbf{F}^0. \tag{2.6}$$

With a strain-controlled homogenization, the macroscopic deformation $\bar{\mathbf{F}}$ and magnetostrictive eigen-deformation \mathbf{F}^0 (deformation gradient associated with eigen-strain) are specified, and the microscale displacement field is

$$\mathbf{u}(\mathbf{X}) = (\bar{\mathbf{F}} - \mathbf{F}^0 - \mathbf{1}) \cdot \mathbf{X} + \mathbf{u}^*(\mathbf{X}), \tag{2.7}$$

where $\mathbf{u}(\mathbf{X})$ is the total microscale displacement and $\mathbf{u}^*(\mathbf{X})$ denotes the locally periodic fluctuating displacement to be solved.

The constitutive relationship for a hyperelastic material can be defined by a strain energy density function W . On the microscale, the work conjugate stress to the deformation gradient is the first Piola–Kirchhoff stress, denoted by \mathbf{P} and given by

$$\mathbf{P}^T(\mathbf{X}) = \frac{\partial W}{\partial \mathbf{F}}, \tag{2.8}$$

$$W = \begin{cases} A_1(\bar{I}_1 - 3) + A_2(\bar{I}_2 - 3) + \frac{k}{2}(J - 1)^2 & \text{if } \mathbf{X} \in \Omega_X^r, \\ \frac{1}{2} \mathbf{E} : \mathbf{C} : \mathbf{E} & \text{if } \mathbf{X} \in \Omega_X^m, \end{cases} \tag{2.9}$$

where $\bar{I}_1 = I_1 I_3^{-2/3}$, $\bar{I}_2 = I_2 I_3^{-2/3}$, $J = I_3^{1/2}$, I_1 , I_2 and I_3 are the first, second and third invariants of the right Cauchy–Green deformation tensor $\mathbf{G} = \mathbf{F}^T \cdot \mathbf{F}$, $\mathbf{E} = (\mathbf{G} - \mathbf{1})/2$ is the Green–Lagrangian strain, \mathbf{C} is the elasticity tensor of magnetostrictive particle, and A_1 , A_2 , and k are material constants of rubber.

For the stress field, the periodicity condition (2.1) also implies

$$\mathbf{P}(X_1, X_2) = \mathbf{P}(X_1 + n_1 \lambda_1, X_2 + n_2 \lambda_2) \tag{2.10}$$

and the macroscale first Piola–Kirchhoff stress is obtained by

$$\bar{\mathbf{P}} = \langle \mathbf{P}(\mathbf{X}) \rangle_{\Omega_X}. \tag{2.11}$$

2.2. Variational equation

With the absence of body force, the equilibrium equation expressed by the first Piola–Kirchhoff stress \mathbf{P} is

$$\nabla_0 \cdot \mathbf{P} = \mathbf{0}, \tag{2.12}$$

$$\nabla_0 \equiv \frac{\partial}{\partial \mathbf{X}}. \tag{2.13}$$

The corresponding variational equation of Eq. (2.12) is

$$\int_{\Omega_X} \delta \mathbf{u} \cdot (\nabla_0 \cdot \mathbf{P}) \, d\Omega = 0, \tag{2.14}$$

where Ω_X is the undeformed configuration (material domain) of the unit microstructure. Integration by parts of (2.14) yields

$$\int_{\Omega_X} \delta \mathbf{F} : \mathbf{P}^T \, d\Omega = \int_{\Gamma_X} \delta \mathbf{u} \cdot \mathbf{P}^T \cdot \mathbf{N} \, d\Gamma, \tag{2.15}$$

where \mathbf{N} is the surface normal on the material boundary Γ_X of unit microstructure in the undeformed configuration. From Eqs. (2.5) and (2.7), it can be shown that

$$\delta \mathbf{F} = \delta \mathbf{F}^*, \tag{2.16}$$

$$\delta \mathbf{u} = \delta \mathbf{u}^*. \tag{2.17}$$

Substituting Eqs. (2.16) and (2.17) into (2.15) yields

$$\int_{\Omega_X} \delta \mathbf{F}^* : \mathbf{P}^T \, d\Omega = \int_{\Gamma_X} \delta \mathbf{u}^* \cdot \mathbf{P}^T \cdot \mathbf{N} \, d\Gamma. \tag{2.18}$$

Further considering the periodicity of the stress \mathbf{P} and displacement $\delta \mathbf{u}^*$, it can be concluded that the right-hand side of (2.18) vanishes for the unit microstructure and this yields

$$\int_{\Omega_X} \delta \mathbf{F}^* : \mathbf{P}^T \, d\Omega = 0, \tag{2.19}$$

subjected to the periodic boundary conditions

$$(\mathbf{u} - \bar{\mathbf{u}})|_{+\Gamma_X^i} = (\mathbf{u} - \bar{\mathbf{u}})|_{-\Gamma_X^i}. \tag{2.20}$$

In Eq. (2.20), $+\Gamma_X^i$ and $-\Gamma_X^i$ denote a surface pair which have the same configuration before and after deformation (Fig. 1), and $\bar{\mathbf{u}}$ is the displacement of a specific reference material point on $+\Gamma_X^i$ and $-\Gamma_X^i$. Usually the surface centroid is chosen as the reference point. Introducing Eq. (2.7) into Eq. (2.20) yields the periodic condition on the fluctuating displacement $\mathbf{u}^*(\mathbf{X})$ as

$$\mathbf{u}^*|_{+\Gamma_X^i} = \mathbf{u}^*|_{-\Gamma_X^i}. \tag{2.21}$$

3. Meshfree discretization

3.1. Interface-enriched reproducing kernel particle method

The reproducing kernel approximation is the foundation of the RKPM [22,23]. The accuracy and rate of convergence of RKPM is determined by the order of reproducing conditions introduced in the reproducing kernel approximation. The reproducing conditions have been employed for coupling of finite element and meshfree methods [32] and for development of a reproducing kernel interpolation function [33]. To deal with problems with material interface in this study, we first consider

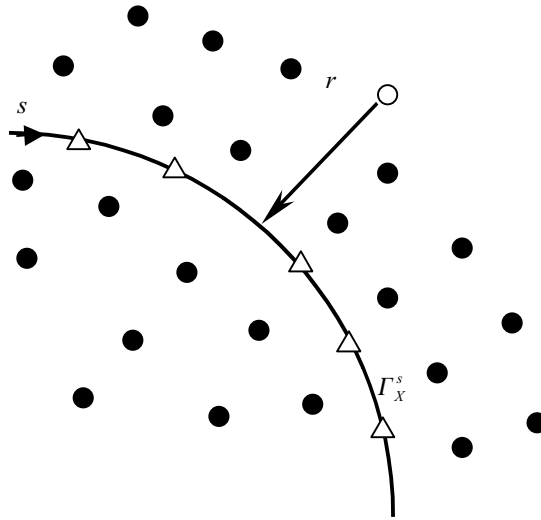


Fig. 2. Discretization of material interface.

the following reproducing kernel approximation of displacement \mathbf{u} , denoted by \mathbf{u}^h , at the material coordinate:

$$u_i^h(\mathbf{X}) = \sum_{I: X_I \notin \Gamma_X^s} \Psi_I(\mathbf{X})d_{il} + \sum_{I: X_I \in \Gamma_X^s} \hat{\Psi}_I(\mathbf{X})\beta_{il}, \tag{3.1}$$

where Γ_X^s is the material interface in the undeformed configuration, $\hat{\Psi}_I(\mathbf{X}(r, s)) = \varphi(r)\phi_I(s)$ is the interface enrichment function [31] defined at the discrete points along Γ_X^s , and r and s are the coordinates normal to and along Γ_X^s , respectively, as shown in Fig. 2. The function $\varphi'(r) \in C^{-1}$ possesses derivative discontinuities on Γ_X^s , and $\phi_I(s)$ is a smooth kernel function along Γ_X^s as demonstrated in Fig. 3. The resulting interface enrichment function $\hat{\Psi}_I$ and $\partial\hat{\Psi}_I/\partial r$ also are plotted in Fig. 3.

The reproducing kernel shape function defined at points $X_I \notin \Gamma_X^s$ is expressed as

$$\Psi_I(\mathbf{X}) = \mathbf{H}^T(\mathbf{X} - \mathbf{X}_I)\mathbf{b}(\mathbf{X})\Phi_a(\mathbf{X} - \mathbf{X}_I), \tag{3.2}$$

where Φ_a is the kernel function and \mathbf{H} is the monomial basis vector defined as

$$\mathbf{H}^T(\mathbf{X} - \mathbf{X}_I) = [1, X_1 - X_{1I}, X_2 - X_{2I}, \dots, (X_2 - X_{2I})^n]. \tag{3.3}$$

The coefficient vector $\mathbf{b}(\mathbf{X})$ in Eq. (3.2) is obtained by imposing the n th order reproducing conditions as follows:

$$\sum_{I: X_I \notin \Gamma_X^s} \Psi_I(\mathbf{X})X_{1I}^i X_{2I}^j + \sum_{I: X_I \in \Gamma_X^s} \hat{\Psi}_I(\mathbf{X})X_{1I}^i X_{2I}^j = X_1^i X_2^j, \quad 0 \leq i + j \leq n. \tag{3.4}$$

By substituting Eq. (3.2) into (3.4), one obtains

$$\mathbf{b}(\mathbf{X}) = \mathbf{M}^{-1}(\mathbf{X})[\mathbf{H}(\mathbf{0}) - \hat{\mathbf{F}}(\mathbf{X})], \tag{3.5}$$

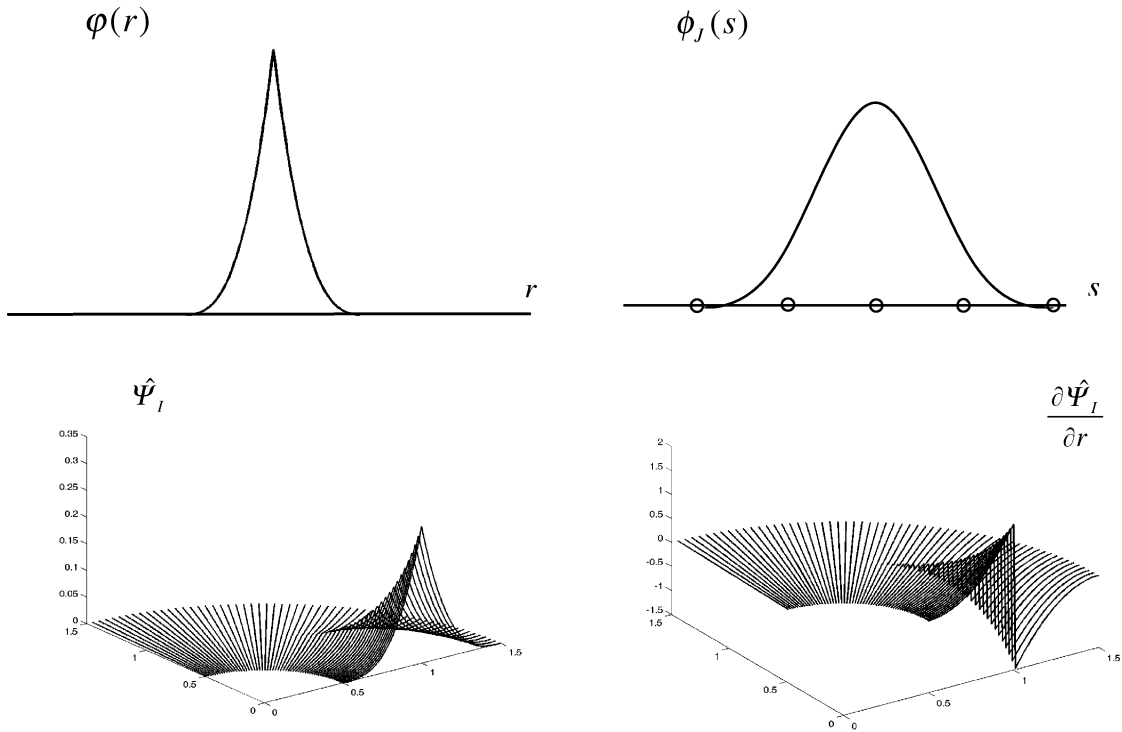


Fig. 3. Interface enrichment function and its derivative.

where

$$\hat{F}(X) = \sum_{I: X_I \in \Gamma_X^s} \hat{\Psi}_I(X) H(X - X_I), \tag{3.6}$$

$$M(X) = \sum_{I: X_I \notin \Gamma_X^s} H(X - X_I) H^T(X - X_I) \Phi_a(X - X_I). \tag{3.7}$$

Finally the reproducing kernel shape function is

$$\Psi_I(X) = H^T(X - X_I) M^{-1}(X) [H(\mathbf{0}) - \hat{F}(X)] \Phi_a(X - X_I). \tag{3.8}$$

Since $\hat{\Psi}_I(X)$ is introduced locally on the material interface, for a point of evaluation X that is not covered by the influence zone of the interface enrichment functions, $\hat{\Psi}_I(X)$ vanishes, and Eq. (3.8) reduces to the standard reproducing kernel shape function.

In summary, the interface-enriched reproducing kernel approximation of Eq. (3.1) can be written in the following form:

$$u_i^h(X) = \sum_I \Psi_I(X) d_{iI} \tag{3.9}$$

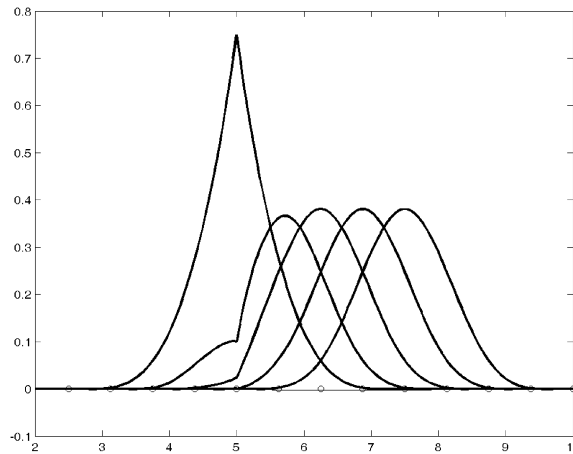


Fig. 4. Coupling between the interface enrichment function and the reproducing kernel function.

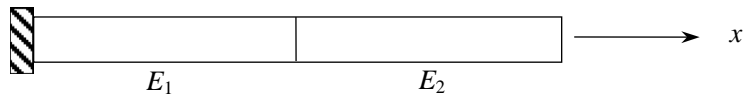


Fig. 5. One-dimensional bi-material rod.

where

$$\Psi_I(\mathbf{X}) = \begin{cases} \hat{\Psi}_I(\mathbf{X}) & \text{for } I : \mathbf{X}_I \in \Gamma_X^s, \\ \mathbf{H}^T(\mathbf{X} - \mathbf{X}_I)\mathbf{M}^{-1}(\mathbf{X})[\mathbf{H}(\mathbf{0}) - \hat{\mathbf{F}}(\mathbf{X})]\Phi_a(\mathbf{X} - \mathbf{X}_I) & \text{otherwise.} \end{cases} \quad (3.10)$$

The coupling between the reproducing kernel shape function and interface enrichment shape function according to Eq. (3.8) is shown in Fig. 4. In this paper, the meshfree method formulated using the above reproducing kernel estimation with interface enrichment is called the I-RKPM.

3.2. Numerical test

3.2.1. One-dimensional bi-material elastic bar

Following [31], the one-dimensional bi-material bar as shown in Fig. 5 is subjected to a body force $b(x) = a_0 + a_1x + a_2x^2 + a_3x^3$. In this study two cases are considered: (1) $a_0 = a_1 = a_2 = a_3 = 0$; (2) $a_0 = 0, a_1 = 25, a_2 = -7.5, a_3 = 0.5$. The elastic moduli of the two materials are $E_1 = 10\,000$ and $E_2 = 1000$. The governing equation of this problem is

$$\frac{d}{dx} \left(E(x) \frac{du}{dx} \right) + b(x) = 0, \quad x \in]0, 10[,$$

$$u(0) = 0, \quad u(10) = 1. \quad (3.11)$$

The elastic constants are

$$E(x) = \begin{cases} E_1, & x \in [0, 5], \\ E_2, & x \in]5, 10]. \end{cases} \quad (3.12)$$

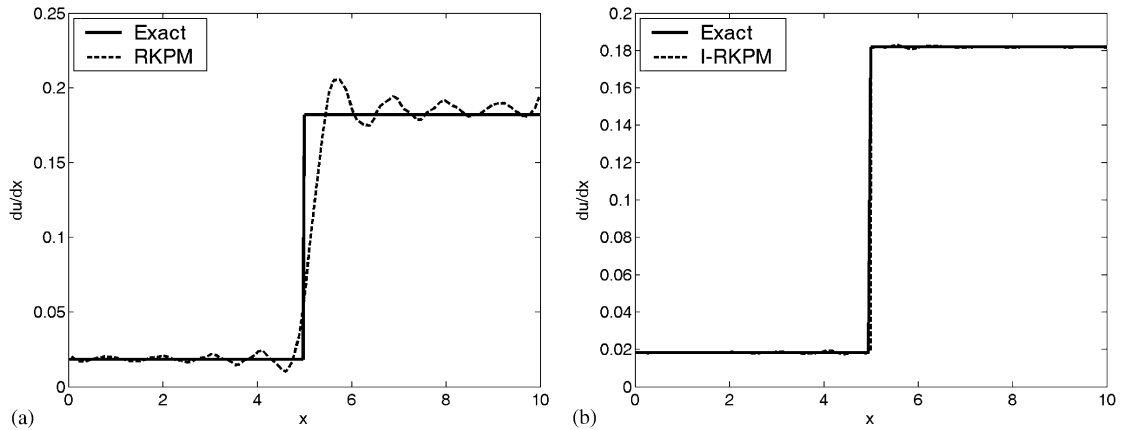


Fig. 6. Strain distribution of 1D rod without body force: (a) RKPM and (b) I-RKPM.

The exact solution of this problem is

$$u(x) = \begin{cases} \frac{1}{E_1}[E_2 Bx + C(x)], & x \in [0, 5], \\ 1 + B(x - 10) + \frac{C(x) - C(10)}{E_2}, & x \in]5, 10], \end{cases} \quad (3.13)$$

$$B = \frac{E_1 E_2 - C(x_b)(E_2 - E_1) - C(10)E_1}{E_2[(E_2 - E_1)x_b + 10E_1]}, \quad (3.14)$$

$$C(x) = - \left(a_0 \frac{x^2}{2} + a_1 \frac{x^3}{6} + a_2 \frac{x^4}{12} + a_3 \frac{x^5}{20} \right), \quad (3.15)$$

where x_b is the separation point of materials 1 and 2, in this example $x_b = 5$.

We analyze this problem using the conventional RKPM and the proposed I-RKPM, both consume the same degrees of freedom in the discretization. Due to the use of smooth kernel, the strain solution obtained by RKPM is highly oscillatory as shown in Fig. 6 for case (1). This deficiency can be corrected with the I-RKPM without additional degrees of freedom in the approximation. Similar behavior is observed in the case of higher order solution as shown in Fig. 7.

3.2.2. Inclusion with eigen-strain in an infinite plate

A circular inclusion with a constant equal-biaxial eigen-strain ϵ^0 is embedded in an infinite matrix as shown in Fig. 8. The exact solution of displacement for this problem is

$$u_r = \begin{cases} C_1 r, & r \leq R, \\ C_1 \frac{R^2}{r}, & r \geq R. \end{cases} \quad (3.16)$$

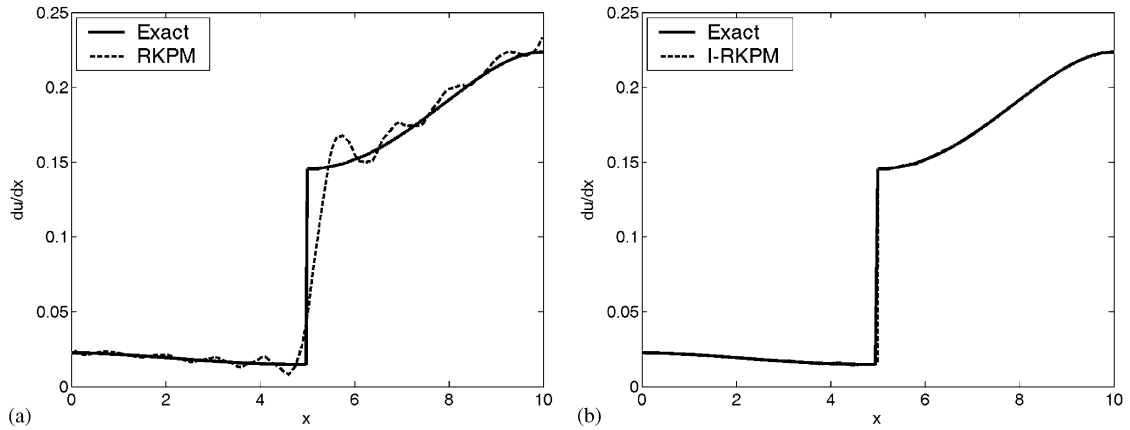


Fig. 7. Strain distribution of 1D rod with body force: (a) RKPM and (b) I-RKPM.

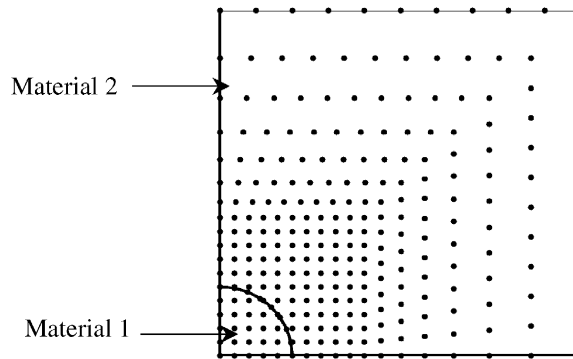


Fig. 8. Discretization of a 2D bi-material plate.

The corresponding radial strain field of this problem is

$$\epsilon_{rr} = \begin{cases} C_1, & r \leq R, \\ -C_1 \frac{R^2}{r^2}, & r \geq R, \end{cases} \tag{3.17}$$

$$C_1 = \frac{(\lambda_1 + \mu_1)\epsilon^0}{\lambda_1 + \mu_1 + \mu_2}, \tag{3.18}$$

where R is the radius of inclusion, λ_i and μ_i are Lamé constants of material phase: $i=1$ for inclusion and $i=2$ for matrix, and ϵ^0 denotes the prescribed constant equal-biaxial eigen-strain in the inclusion.

The material constants used for this example are $\lambda_1 = 497.16$, $\mu_1 = 390.63$, $\lambda_2 = 656.79$, and $\mu_2 = 338.35$. The equal-biaxial eigen-strain ϵ^0 of the inclusion is given as 0.01. Due to the symmetry, only one-quarter of the domain is analyzed as shown in Fig. 8, where each side of the quarter domain is of length 5, and the radius of the inclusion is $R = 1$. Exact displacement boundary conditions

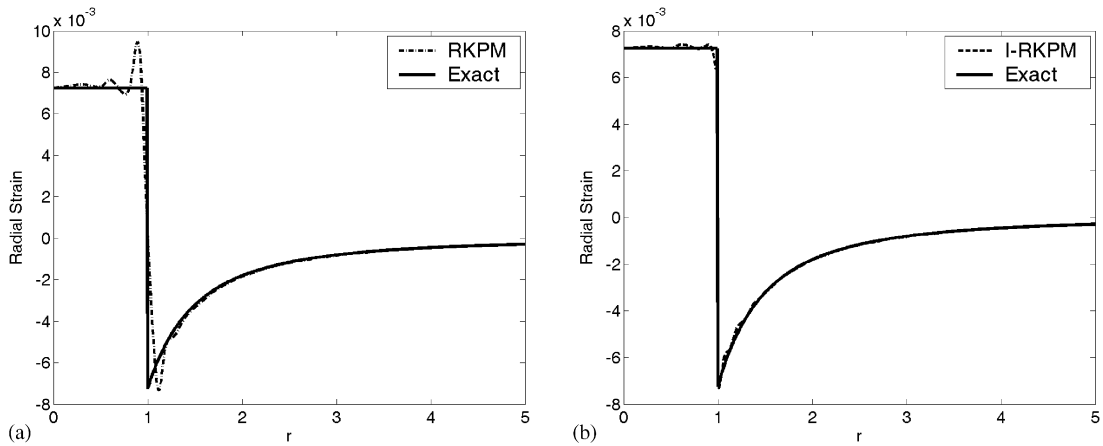


Fig. 9. Comparison of radial strain: (a) RKPM and (b) I-RKPM.

are imposed on the top and right surfaces, and symmetric boundary conditions are imposed on the bottom and left surfaces. The solutions of radial strain using RKPM and I-RKPM are compared in Fig. 9, and improved accuracy is obtained using the proposed I-RKPM.

4. Discretization of homogenization variational equation

For a given value of macroscale deformation $\bar{\mathbf{F}}$ and an eigen-deformation \mathbf{F}^0 , the microscale displacement field is approximated by

$$u_i^h(\mathbf{X}) = (\bar{F}_{ij} - F_{ij}^0 - \delta_{ij})X_j + \sum_{I=1}^{NP} \Psi_I(\mathbf{X})d_{iI}^*, \tag{4.1}$$

where Ψ_I are the interface-enriched reproducing kernel shape functions of Eq. (3.10), NP is the total number of discrete particles, and d_{iI}^* are coefficients of the local fluctuating periodic displacements to be solved. Introducing Eq. (4.1) into the linearization form of Eq. (2.19), the incremental discrete equation is obtained as

$$(\mathbf{K}^M + \mathbf{K}^G) \Delta \mathbf{d}^* = -\mathbf{f}^{\text{int}}, \tag{4.2}$$

$$\mathbf{K}_{IJ}^M = \int_{\Omega_0} \mathbf{B}_I^{M^T} \mathbf{D} \mathbf{B}_J^M d\Omega, \tag{4.3}$$

$$\mathbf{K}_{IJ}^G = \int_{\Omega_0} \mathbf{B}_I^{G^T} \mathbf{T} \mathbf{B}_J^G d\Omega, \tag{4.4}$$

$$\mathbf{f}_I^{\text{int}} = \int_{\Omega_0} \mathbf{B}_I^{G^T} \Sigma d\Omega, \tag{4.5}$$

where

$$\mathbf{B}_I^G = \begin{bmatrix} \Psi_{I,1} & 0 \\ 0 & \Psi_{I,2} \\ \Psi_{I,2} & 0 \\ 0 & \Psi_{I,1} \end{bmatrix}, \quad \Psi_{I,i} = \frac{\partial \Psi_I}{\partial X_i}, \quad (4.6)$$

$$\mathbf{B}_I^M = \begin{bmatrix} \Psi_{I,1} & 0 \\ 0 & \Psi_{I,2} \\ \Psi_{I,2} & \Psi_{I,1} \end{bmatrix}, \quad (4.7)$$

$$\mathbf{D} = \begin{bmatrix} D_{1111} & D_{1122} & D_{1112} \\ D_{2211} & D_{2222} & D_{2212} \\ D_{1211} & D_{1222} & D_{1212} \end{bmatrix}, \quad (4.8)$$

$$\mathbf{T} = \begin{bmatrix} S_{11} & 0 & S_{12} & 0 \\ 0 & S_{22} & 0 & S_{21} \\ S_{21} & 0 & S_{22} & 0 \\ 0 & S_{12} & 0 & S_{11} \end{bmatrix}, \quad (4.9)$$

$$\boldsymbol{\Sigma}^T = [P_{11} \quad P_{22} \quad P_{21} \quad P_{12}], \quad (4.10)$$

where $D_{ijkl} = F_{ip} F_{jq} C_{pqkl}^s$, $\mathbf{C}^s = \partial^2 W / \partial \mathbf{E} \partial \mathbf{E}$ is the material response tensor, \mathbf{E} is the Green–Lagrangian strain, and \mathbf{S} is the second Piola–Kirchhoff stress $\mathbf{S} = \mathbf{P} \cdot \mathbf{F}^{-T}$.

In the solution of the incremental equation (4.2), the periodic boundary conditions (Eq. (2.21)) are imposed on $\Delta \mathbf{d}^*$. These periodic conditions of the fluctuating displacement field $\Delta \mathbf{d}^*$ can be imposed by enforcing the particle pair on the opposite boundaries of the unit cell to share the same degrees of freedom.

At the end of nonlinear calculation, the volume average of the first Piola–Kirchhoff stress is obtained by

$$\bar{\mathbf{P}} \equiv \langle \mathbf{P} \rangle \equiv \frac{1}{V} \int_{\Omega_0} \mathbf{P}(\mathbf{X}) \, d\Omega. \quad (4.11)$$

The corresponding homogenized Cauchy stress $\bar{\boldsymbol{\sigma}}$ can be obtained from $\bar{\mathbf{P}}$ by transformation:

$$\bar{\boldsymbol{\sigma}} = \frac{1}{\bar{J}} \bar{\mathbf{F}} \cdot \bar{\mathbf{P}}, \quad \bar{J} = \det[\bar{\mathbf{F}}]. \quad (4.12)$$

5. Numerical examples

In this study we consider a unit microstructure with a 21% volume fraction. The rubber material is modeled by a Moony–Rivlin strain energy density function (Eq. (2.9)) with $A_1 = 1.69 \text{ kg/cm}^2$, $A_2 = 0.7 \text{ kg/cm}^2$, and bulk modulus $k = 10^4 \text{ kg/cm}^2$. A relatively large elastic constant $E = 500 \text{ kg/cm}^2$ is used for the inclusion. In this example, the dimension of unit cell is $4 \text{ cm} \times 4 \text{ cm}$, the radius of the inclusion is 1.0342 cm such that the volume fraction is 21%.

As shown in Fig. 10, the unit microstructure is discretized by a set of uniformly distributed points, and the interface solution is enhanced by interface enrichment functions following Eqs. (3.9) and (3.10). It can be seen that with the proposed approach the discretization of bi-material microstructure is quite straightforward.

5.1. Uniaxial tension test

We first analyze the tension response of MPFE. To evaluate the effect of magnetostrictive eigen-strain (magnetostriction) to the behavior of MPFE, various degrees of magnetostriction, ranging from 1 to 10%, are considered. In the uniaxial tension test the macroscopic deformation is given as

$$\bar{\mathbf{F}}_{\text{tension}} = \begin{bmatrix} 1.4 & 0.0 \\ 0.0 & 0.714 \end{bmatrix}. \tag{5.1}$$

Note that MPFE is assumed nearly incompressible, and the prescribed macroscopic deformation (5.1) is volume preserving. The magnetostriction of the inclusion is purely dilatational with volume preserving. As an example, the deformation gradient corresponding to a 3% magnetostriction is given by

$$\mathbf{F}^0 = \begin{bmatrix} 1.03 & 0.0 \\ 0.0 & 0.97 \end{bmatrix}. \tag{5.2}$$

Fig. 11 shows the local fluctuating deformation and overall combined deformation fields for the case without magnetostriction. The local fluctuating deformation and overall combined deformation fields for the case with a 3% magnetostriction are plotted in Fig. 12. The responses of homogenized axial Cauchy stress versus axial stretch are compared to experimental data [19]

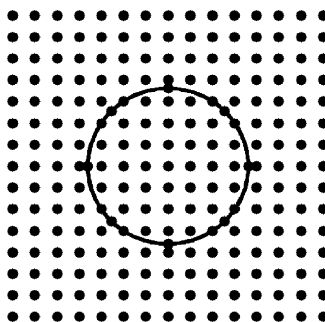


Fig. 10. Meshfree discretization of unit microstructure.

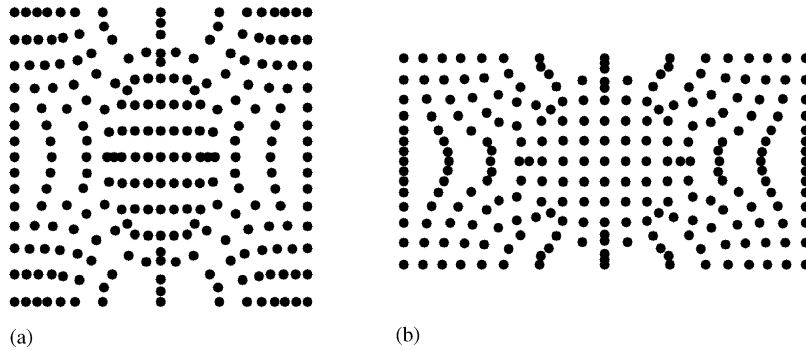


Fig. 11. Deformation of uniaxial tension without magnetostriction effect: (a) local fluctuating deformation, and (b) microscopic total deformation.

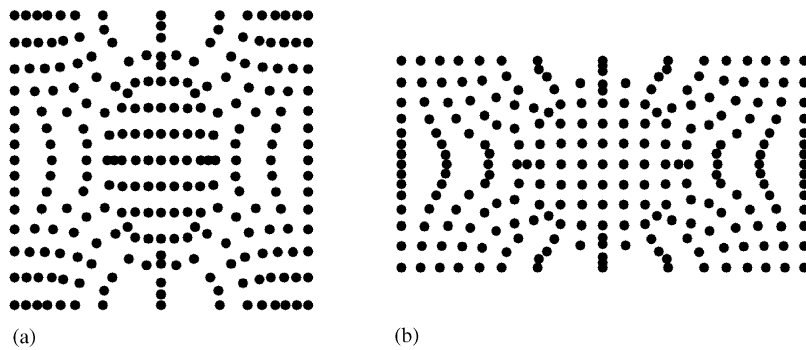


Fig. 12. Deformation of uniaxial tension with 3% magnetostriction: (a) local fluctuating deformation, and (b) microscopic total deformation.

in Fig. 13, which shows that the existence of magnetostriction has noticeable influence on the overall tension behavior of MPFE.

5.2. *Simple shear test*

For the simple shear test the macroscopic deformation is given by

$$\bar{\mathbf{F}}_{\text{shear}} = \begin{bmatrix} 1.0 & 1.0 \\ 0.0 & 1.0 \end{bmatrix}. \tag{5.3}$$

Similar to the tension test, we also consider the magnetostriction ranging from 1 to 10%. Figs. 14 and 15 show the local fluctuating deformation and overall combined deformation fields for the cases without and with a 3% magnetostriction, respectively. Fig. 16 shows the homogenized stress–strain curves for the simple shear case. Since the magnetostriction is dilatational, it has little effect on the overall behavior of MPFE in the simple shear deformation.

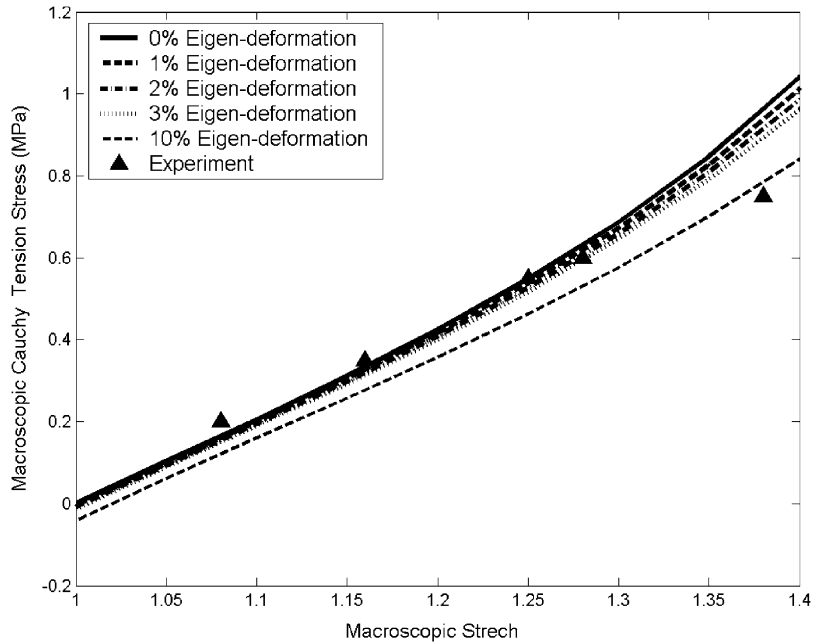


Fig. 13. MPFE Cauchy stress versus axial stretch in uniaxial tension.

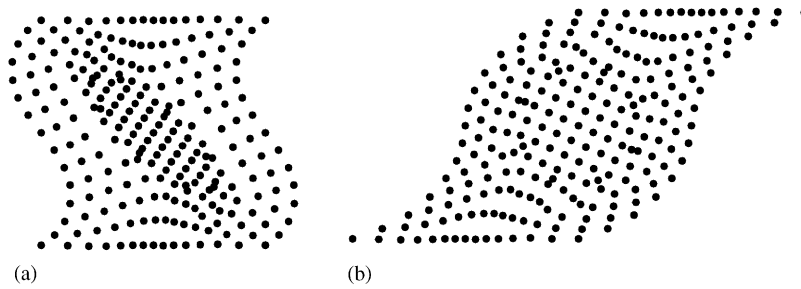


Fig. 14. Displacement fields without magnetostriction effect for simple shear test: (a) local fluctuating deformation, and (b) microscopic total deformation.

6. Conclusion

In this paper we present the computational formulation for analyzing the microscopic and macroscopic behavior of magnetostrictive particle-filled elastomer (MPFE). For effective modeling of MPFE unit microstructure, we employed a Galerkin meshfree method based on a reproducing kernel approximation. The interface conditions between rubber and magnetostrictive particle components are embedded in an interface-enriched reproducing kernel approximation for the displacement field. The proposed interface-enriched reproducing kernel approximation is constructed by coupling the reproducing kernel shape function and the interface enrichment shape function via the reproducing

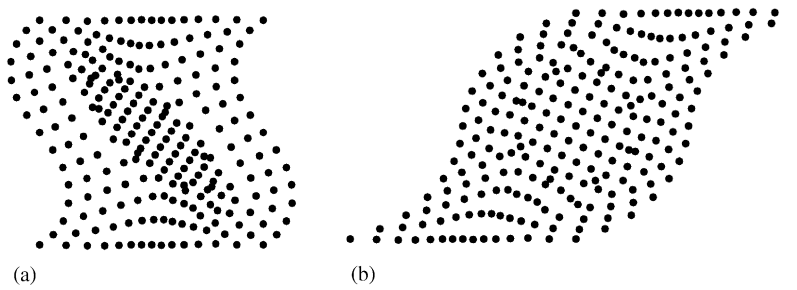


Fig. 15. Displacement fields with 3% magnetostriction for simple shear test: (a) local fluctuating deformation, and (b) microscopic total deformation.

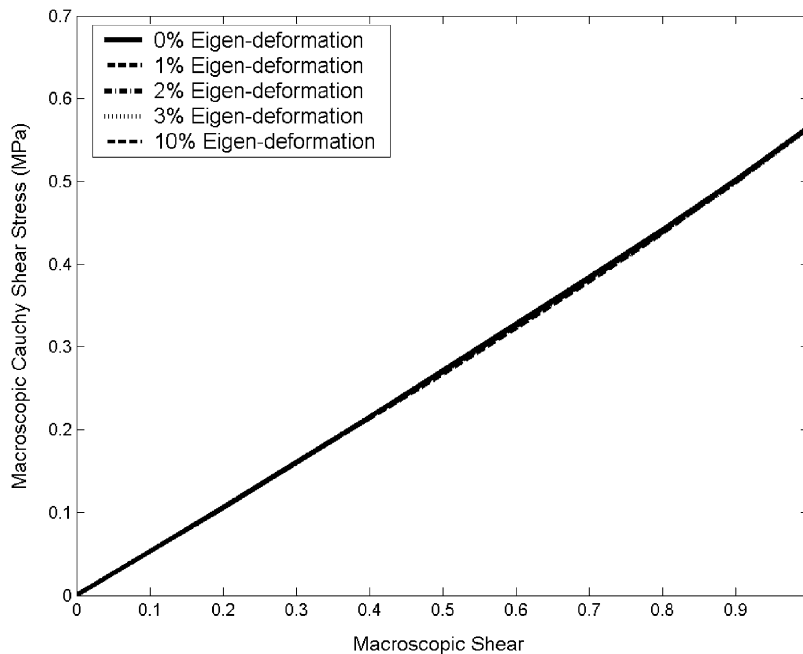


Fig. 16. Cauchy shear stress versus shear strain.

conditions. This approach significantly improves the near-interface solution of the reproducing kernel approximation without using additional degrees of freedom in the approximation of displacements.

We also presented a homogenization variational equation for obtaining microscale deformation of MPFE for general large deformation conditions. The microscale deformation is composed of the macroscale deformation, the local fluctuating deformation, and the magnetostrictive eigen-deformation. The local displacement is approximated using the proposed interface-enriched reproducing kernel approximation and thus the meshing complexity of MPFE microstructure is simplified. Using the proposed method, the effective nonlinear stress–strain relations of MPFE uniaxial tension and simple shear deformation have been obtained. The effects of the magnetostriction on the overall MPFE

behavior have also been analyzed. The results show that the magnetostrictive properties in the particle inclusions have stronger influence on the MPFE behavior under dilatational deformation.

Acknowledgements

The support of this work by National Science Foundation under the grant CMS 00-84629 to UCLA and The University of Iowa is greatly acknowledged.

References

- [1] S. Bednarek, The giant magnetostriction in ferromagnetic composites within an elastomer matrix, *Appl. Phys. A* 68 (1999) 63–67.
- [2] M.R. Jolly, J.D. Carlson, B.C. Munoz, A model of the behavior of magnetorheological materials, *Smart Mater. Struct.* 5 (1996) 607–614.
- [3] T. Mura, *Mechanics of Defects in Solids*, Nijhoff, The Hague, 1987.
- [4] C.W. Nan, Effective magnetostriction of magnetostrictive composites, *Appl. Phys. Lett.* 72 (1998) 2897–2899.
- [5] Y. Chen, J.E. Snyder, C.R. Schwichtenberg, K.W. Dennis, D.K. Falzgraf, R.W. McCallum, D.C. Jiles, Effect of the elastic modulus of the matrix on magnetostrictive strain in composites, *Appl. Phys. Lett.* 74 (1999) 1159–1161.
- [6] J.S. Bergström, M.C. Boyce, Mechanical behavior of particle filled elastomers, *Rubber Chem. Technol.* 72 (1999) 633–656.
- [7] S. Govindjee, J. Simo, A micro-mechanically based continuum damage model for carbon black-filled rubbers incorporating Mullins effect, *J. Mech. Phys. Solids* 39 (1991) 87–112.
- [8] M.P. Bendsoe, C.A. Soares Mota (Eds.), *Topology Design of Structures*, Kluwer Academic Publishers, Dordrecht, 1993.
- [9] E. Sanchez-Palebnicia, A. Zaoui (Eds.), *Homogenization Techniques for Composite Media*, Springer, Berlin 1987.
- [10] Y.L. Shen, M. Finot, A. Needleman, S. Suresh, Effective elastic response of two-phase composites, *Acta Metall. Mater.* 42 (1994) 77–97.
- [11] P.M. Suquet, Elements of homogenization for inelastic solid mechanics, in: E. Sanchez-Palebnicia, A. Zaoui (Eds.), *Homogenization Techniques for Composite Media*, Springer, Berlin, 1987, pp. 193–278.
- [12] C.C. Swan, Techniques for stress- and strain-controlled homogenization of inelastic periodic composites, *Comput. Meth. Appl. Mech. Eng.* 117 (1994) 249–267.
- [13] J.C. Michel, H. Moulinec, P.M. Suquet, Effective properties of composites with periodic microstructure: a computational approach, *Comput. Meth. Appl. Mech. Eng.* 172 (1999) 109–143.
- [14] C. Pellegrino, U. Galvanetto, B.A. Schrefler, Numerical homogenization of periodic composite materials with non-linear material response, *Int. J. Numer. Methods Eng.* 46 (1999) 1609–1637.
- [15] H. Moulinec, P.M. Suquet, A numerical method for computing the mechanical properties with complex microstructure, *Comput. Meth. Appl. Mech. Eng.* 157 (1997) 69–94.
- [16] S. Jansson, Homogenized nonlinear constitutive properties and local stress concentration for composites with periodic internal structure, *Int. J. Solids Struct.* 29 (1992) 2181–2200.
- [17] L.H. Craig, Three-dimensional finite element analysis of plastic deformation in a whisker-reinforced metal matrix composite, *J. Mech. Phys. Solids* 40 (1992) 991–1008.
- [18] J. Llorca, S. Suresh, A. Needleman, An experimental and numerical study of cyclic deformation in metal-matrix composites, *Metall. Trans. A* 23A (1992) 919–934.
- [19] L. Mullins, N.R. Tobin, Stress softening in rubber vulcanizates, Part I: use of a strain amplification factor to describe the elastic behavior of filler-reinforced vulcanized rubber, *J. Appl. Polym. Sci.* 9 (1965) 2993–3009.
- [20] T. Belytschko, Y.Y. Lu, L. Gu, Element-free Galerkin methods, *Int. J. Numer. Methods Eng.* 37 (1994) 229–256.
- [21] Y.Y. Lu, T. Belytschko, L. Gu, A new implementation of the element free Galerkin method, *Comput. Methods Appl. Mech. Eng.* 139 (1994) 397–414.

- [22] W.K. Liu, S. Jun, Y.F. Zhang, Reproducing kernel particle methods, *Int. J. Numer. Methods Fluids* 20 (1995) 1081–1106.
- [23] W.K. Liu, S. Jun, S. Li, J. Adee, T. Belytschko, Reproducing kernel particle methods structural dynamics, *Int. J. Numer. Methods Eng.* 38 (1995) 1655–1679.
- [24] J.S. Chen, C. Pan, C.T. Wu, W.K. Liu, Reproducing kernel particle methods for large deformation analysis of nonlinear structures, *Comput. Methods Appl. Mech. Eng.* 139 (1996) 195–227.
- [25] J.S. Chen, H.P. Wang, New boundary condition treatments for meshless computation of contact problems, *Comput. Methods Appl. Mech. Eng.* 187 (2000) 441–468.
- [26] I. Babuska, J.M. Melenk, The partition of unity method, *Int. J. Numer. Methods Eng.* 40 (1997) 727–758.
- [27] J.M. Melenk, I. Babuska, The partition of unity finite element method: basic theory and applications, *Comput. Methods Appl. Mech. Eng.* 139 (1996) 289–314.
- [28] C.A.M. Duarte, J.T. Oden, A h-p adaptive method using clouds, *Comput. Methods Appl. Mech. Eng.* 139 (1996) 237–262.
- [29] C.A.M. Duarte, J.T. Oden, Hp clouds—a meshless method to solve boundary-value problems, *Numer. Methods Partial Differential Equations* 12 (6) (1996) 673–705.
- [30] L.W. Codes, B. Moran, Treatment of material discontinuity in the element-free Galerkin method, *Comput. Methods Appl. Mech. Eng.* 139 (1996) 75–89.
- [31] Y. Krongauz, T. Belytschko, EFG approximation with discontinuous derivatives, *Int. J. Numer. Methods Eng.* 41 (1998) 1215–1233.
- [32] A. Huerta, S. Fernández-Méndez, Enrichment and coupling of the finite element and meshless methods, *Int. J. Numer. Methods Eng.* 48 (2000) 1615–1636.
- [33] J.S. Chen, W. Han, Y. You, X. Meng, Reproducing kernel interpolation without finite element enrichment, *Int. J. Numer. Methods Eng.* 56 (2003) 935–960.